Analysis of ultracentrifugation interference patterns with image digitizer: Application to molecular weight determination of SRM 1478 polystyrene†

Francis W. Wang and Frank L. McCrackin
Polymer Science and Standards Division, National Bureau of Standards, Washington, DC 20234, USA
(*Received* 22 *February* 1983)

A new method for the analysis of ultracentrifugation interference patterns with the use of a commercial image digitizer is given. The application of the method to the sedimentation equilibrium data for SRM 1478 polystyrene leads to a weight-average molecular weight of 37 400 g mol^{-1} having a sample standard deviation of 0.7% and an expected systematic error limit of 2%.

Keywords Image digitization; Rayleigh interference pattern; sedimentation equilibrium; SRM 1478 polystyrene; ultracentrifugation; weight-average molecular weight

INTRODUCTION

Standard Reference Material (SRM) 1478, issued by the National Bureau of Standards, is a linear polystyrene with relatively narrow distribution in molecular weight. In this paper, we describe the determination of its certificate value of weight-average molecular weight by ultracentrifugation. To analyse the ultracentrifugation data recorded in the form of a Rayleigh interference pattern on a photographic plate, we have developed an automated photographic plate analysis procedure utilizing a commercial image digitizer. This procedure is also described here.

EXPERIMENTAL

Materials

The polystyrene used was SRM 1478, an anionically polymerized linear polystyrene. The solvent was cyclohexane, distilled from Eastman* practical grade cyclohexane over the boiling point range of 80.9°–91.1°C.

Ultracentrifuge

The experiments were performed with a Spinco Model E ultracentrifuge equipped with a temperature control system and the multislit Rayleigh interferometer of Svenssen[1,2]. In the application of Svenssen's method to the Spinco Model E ultracentrifuge, the only modification to the present commercial optical system is the replacement of the single light source slit by a multiple slit having specific dimensions. The multiple slit was made by the same master negative used by Billick and Bowen in the manner described by them[2]. The arrangement of the multiple slit was also essentially the same as theirs: the multiple slit was placed on top of the dust cover of the light source, separated from the light source by a piece of heat-reflecting glass (Bausch and Lomb, Type No. 90-21); an interference filter having a peak wavelength of 5460 Å, in turn, was mounted on top of the multiple slit. The only modification made to their original arrangement was to effect additional cooling of the multiple slit by passing a swift stream of air under the heat-reflecting glass[3].

The optical system was aligned in the manner described by Richards and coworkers[4,5]. For initial positioning of the height of the light source, the multiple slit was replaced by a narrow, rectangular single slit formed by the edges of two razor blades clamped on the top of a dust cover of the light source. Relative to the light housing, this single slit had the same height as the multiple slit and had its longer edges oriented normal to those of the multiple slit, when the respective dust covers holding these slits were placed on the light source housing. The camera lens was focused half-way through the cell. A symmetrical aperture with slits of 0.24 mm wide was used. The thickness of the double-sector centrepieces in the direction of the optical path was measured with a micrometer with very narrow jaws (L. S. Starret Company, Model No. 486-1 IN) on tightened cells.

The Rotor Temperature Indicator and Control (RTIC) unit of the Model E ultracentrifuge was used to indicate the temperature of the rotor. The thermistor of the RTIC unit was calibrated with a thermocouple. The hot junction of the thermocouple was located in the thermometer holder, which was placed in a rotor hole. Calibration was performed with the stationary rotor and mercury cup at their respective operational positions, the thermocouple leads being brought into the rotor chamber through its upper u.v. window port. The RTIC unit was not used to control the rotor temperature, since the heating from the unit was found to destroy the concentration gradient in the solution. Instead, the fluid from a bath equipped with a proportional temperature controller was circulated through the refrigeration liner around the rotor chamber to control the rotor temperature.

* Certain commercial equipment, instruments, or materials are identified in this paper in order adequately to specify the experimental procedure. Such identification does not imply recommendation or endorsement by the National Bureau of Standards, nor does it imply that the materials or equipment identified are necessarily the best available for the purpose.

† This article is not subject to U.S. Copyright

0032-3861/83/121541-06$03.00

Synthetic boundary experiment

The initial concentration of solute c_0 was determined with a double-sector synthetic boundary cell placed in an An-D rotor. An interference cell was assembled with a 12 mm, charcoal-filled epon, double-sector synthetic boundary centrepiece and sapphire windows. An appropriately weighted counterbalance of the type for the Schlieren optical system was used, since the counterbalance for the interference optical system was found to pass insufficient light for registering the reference marks. In the right-hand compartment (screw ring facing the worker) of the interference cell was placed 0.15 ml of solution and in the other 0.42 ml of solvent. Synthetic boundary and sedimentation equilibrium experiments were both performed at 35.0°C, since the refractive index increment dn/dc varies with temperature. Sufficient time was allowed to pass before evacuating the chamber to permit temperature equilibration of the cell and the rotor. As soon as the evacuation of the chamber was started, the rotor was accelerated with a current of 6 A until the synthetic boundary was formed and then with a current of 9 A until the rotor speed of 20 000 rpm was attained. The drive voltage was then set at 40 V suggested by the Model E Instruction Manual to give a rotor speed of 20 000 rpm. A photograph of the interference pattern was taken on a Kodak spectrographic type II-G plate when the menisci became superimposed. The speed of the rotor was then reduced on fast brake and diffusion allowed to occur at 5200 rpm. When the fringes in the boundary region became resolvable on the viewing screen, another photograph of the interference pattern was taken. At the conclusion of the centrifugation the cell was removed from the rotor, the solution was withdrawn from the compartment, and finally 0.30 ml of the solvent was added to the compartment which had been thoroughly rinsed with the solvent. The rotor with the cell properly replaced was then brought to 35.0°C and 20 000 rpm and the baseline picture was taken.

Sedimentation equilibrium experiment

The sedimentation equilibrium experiment was performed with an interference cell assembled with a 12 mm, Kel-F, double-sector centrepiece and sapphire windows. An appropriately weighted counterbalance for the Schlieren optical system was used. The solution was overlapped by solvent at both ends to give interfaces that were distinct from those in the reference compartment. Thus, to one compartment of the cell were added 0.005 ml of distilled water and 0.125 ml of solvent and to the other compartment were added 0.015 ml of distilled water and 0.100 ml of solution to form a column of approximately 3 mm height. An An-D rotor in which the filled cell and the counterbalance were properly placed was mounted in the chamber and allowed to equilibrate to 35.0°C. The rotor was then accelerated to the operating speed of 10 000 rpm and an interference photograph was taken immediately on a Kodak spectrographic plate, type II-G. To ascertain the attainment of equilibrium, interference photographs were taken at intervals on Kodak Metallographic plates. The positions of a few fringes near the cell extremities were then measured with a comparator. When these values were constant the experiment was terminated, at least 22 h after the operating speed was attained. After the rotor had stopped, the compartment of the cell containing the solution was rinsed with the solvent and filled with 0.15 ml of solvent as described for the synthetic boundary experiment. The rotor with the cell properly replaced was then brought to 35.0°C and 10 000 rpm and the baseline picture was taken.

Partial specific volume

The partial specific volume of SRM 1478 in cyclohexane at 35.0°C was determined with the use of a Mettler/PAAR Precision Digital Density Meter (DMA 60 Processing Unit and DMA 601 HP External Measuring Cells, distributed by Mettler Instrument Corporation). Each time the density of a polystyrene solution was determined, the density meter was calibrated with a heptane sample and a xylene sample. The densities of the heptane sample and the xylene sample were determined in two ways: with the use of a pycnometer and with the use of the Mettler/Paar Precision Digital Density Meter which was calibrated with air and a primary xylene standard. (The density of the primary standard was determined by a hydrostatic method in the manner described by Bowman and coworkers[6,7].) The differences between the density readings obtained in these two ways were 50 ppm and 20 ppm for the xylene sample and heptane sample, respectively.

Digitizing and analysis of interference photograph

The optical density profiles of the interference photographs were obtained with the use of a Boller and Chivens PDS Microdensitometer System. *Figure 1* shows a typical photograph. The interference photograph was placed on the microdensitometer stage such that the image of the outer reference edge was parallel to the x-axis of the stage. In measuring an interference photograph, the densitometer moves along a 2 cm long scan line in the x-direction at various y-distances from the image of the outer reference edge. (For brevity, the phrase 'the image of' will be omitted hereafter.) Moving along each of the scan lines, the densitometer measures at 21 μm intervals the optical density of a 21 μm-square scan area of the interference photograph.

For the determination of the position of the outer or the inner reference edge (A–A′ or D–D′ on *Figure 1*) on an interference photograph, optical density readings along 40 scan lines, symmetrically located about the reference edge at 21 μm intervals, were measured and recorded as a file on a magnetic tape. Similarly for each of the menisci (B–B′ and C–C′), optical density readings along 30 scan lines, symmetrically located about the meniscus at 21 μm intervals, were recorded. For the evaluation of an interference pattern, optical density readings along scan lines located between the top and the bottom menisci (region between B–B′ and C–C′) at 21 μm intervals were recorded.

These files on magnetic tapes were analysed by computer to locate the y-positions of the reference lines, menisci, and the displacement of the fringes.

The reference lines are represented by a sharp change of optical density, occurring over about five scans. In order to reduce the errors in readings of optical densities, the readings of each scan were averaged in groups of ten. Next, for each value of x, the optical densities for five scans on each side of the reference line were averaged to find the plateau values of the optical density. Finally for each x, the optical densities for three scans centred on the reference line were fitted to a linear function of y. From this line, the value of y for which the optical density is

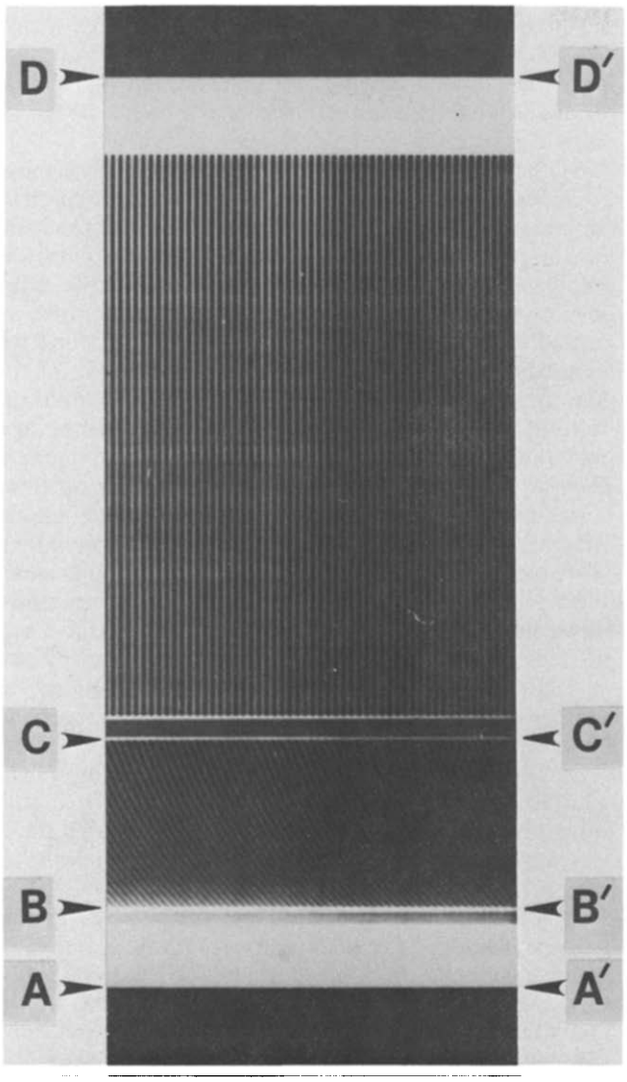

Figure 1 Typical ultracentrifugation Rayleigh interference pattern. A–A′ is the inner reference edge, B–B′ and C–C′ are the menisci bounding the curved fringes due to the solution. The straight fringes between the meniscus C–C′ and the upper reference edge, D–D′, are due to solvent

equal to the average of the optical densities of the plateau regions, one from each side of the reference line, was calculated and taken as the position of the reference line.

If the photograph had been aligned exactly on the microdensitometer stage, the positions of the reference lines would be independent of x. However, the positions of the reference lines in general showed a small variation with x-position due to a tilt in alignment of the photographic plate. The tilt was also observed for the menisci. The angles of tilt were computed for the two reference lines and two menisci of each photographic plate and were averaged. All measurements of the fringes were corrected for this tilt.

Each meniscus corresponds to a minimum in the optical density along the y-direction on the photographic plate. First, as for the reference lines, the readings for each scan were averaged in groups of ten. For each value of x, seven values of optical density for y-values around the meniscus were fitted to a quadratic equation, and the y-value for the minimum of the optical density was computed from the equation and taken as the position of the meniscus. From the variation of the position of the meniscus with x, the tilt of the photographic plate was computed for each meniscus.

The displacement *versus* y of the fringes (hereafter referred to as fringe displacement) in the region between B–B′ and C–C′ of *Figure 1* is to be determined. At each y-position the optical density I of the photographic plate is given approximately by

$$I = E\sin(2\pi x/S + \phi) + F \tag{1}$$

where F is the background intensity, S is the period of the fringes (or the distance between consecutive maxima in optical density), and ϕ is the phaseshift.

The phaseshift ϕ will vary with y but the fringe period S will remain constant. The value of the fringe period S was first measured from the photograph. Then equation (1) was fitted to the values of I at each y, and values of E, ϕ, F and the standard deviation of the fit were determined for all the scans of the plate. In order to increase the accuracy of S, the fitting was repeated for a number of assumed values of S, and the value of S that gave the minimum standard deviation was chosen. This chosen value of S was used to determine the phaseshift as a function of y.

Let the values of ϕ be ϕ_1 and ϕ_2 for scans at the positions y_1 and y_2, respectively. Then the change in fringe displacement is given by

$$\Delta D = S(\phi_2 - \phi_1)/2\pi \tag{2}$$

Therefore, fringe displacements (relative to the fringe displacement at some arbitrary y-position) are determined at various y-positions.

Determination of initial concentration from synthetic boundary patterns

The concentration of solute c may be expressed in terms of the number of fringes J, which is related to c by the equation

$$J = a^* c(\mathrm{d}n/\mathrm{d}c)/\lambda^* \tag{3}$$

where $(\mathrm{d}n/\mathrm{d}c)$ is the refractive index increment, a^* is the thickness of the solution column in the direction of the optical path, and λ^* is the wavelength of the light used. For the measurement of J_0, the initial concentration of solute in terms of the number of fringes, the whole number of fringes was determined from the interference pattern obtained after resolution of the boundary and the remaining fractional fringe from the pattern photographed immediately after superposition of the menisci. The fringe displacement of the baseline interference pattern (obtained when both cell compartments were filled with the solvent) varies with the radial position in the cell because of artifacts such as strains or tilts of the cell windows. Therefore, this baseline fringe displacement at each radial position was subtracted from the fringe displacement of the interference pattern used to calculate the fractional fringe.

To calculate the fractional fringe, the fringe displacement D was plotted vs. the radial position r. Using the plot thus obtained, we delete from the data the D values for the positions too close to the menisci or the boundary for which the fringes were distorted. The remaining data were then fitted by the least-squares method to the equation

$$D = c_1 r_1^* + c_2 r_2^* + c_3 r \tag{4}$$

where r_1^* is unity and r_2^* is zero for the part of the fringe pattern between the boundary and the inner meniscus while r_1^* is zero and r_2^* is unity for the part between the boundary and the outer meniscus. The fractional fringe was then given by the fractional part of the quantity $(c_2 - c_1)/S$, where S is the fringe period determined from the pattern photographed immediately after superposition of the menisci. And, finally, J_0, the value of c_0 in number of fringes, was obtained by multiplying the total number of fringes by the factor (a_c^*/a_s^*) where a_c^* and a_s^* are, respectively, the thickness in the direction of the optical path for the centrepiece used in the sedimentation equilibrium experiment and the thickness for the centrepiece used in the synthetic boundary experiment.

Molecular weight from sedimentation equilibrium pattern

The weight average molecular weight M_w of the solute was determined with the use of the equation[8]

$$\frac{c_b - c_a}{\lambda c_0} = M_w^* = M_w - B_{ls} M_w^2 c_0 + \dots \quad (5)$$

with

$$\lambda = (1 - \bar{v}\rho_0)\omega^2(r_b^2 - r_a^2)/(2RT) \quad (6)$$

where M_w^* is the apparent weight-average molecular weight, c_b and c_a are the equilibrium solute concentrations at the bottom and the top of the solution column, respectively, B_{ls} is the light scattering second virial coefficient, $\bar{v}$ is the partial specific volume of the solute, ρ_0 is the density of the solvent, R and T are the gas constant and the absolute temperature, ω is the angular velocity of the rotor, and r_b and r_a are the radial distances to the bottom and the top of the solution column, respectively. Since the fringe pattern does not extend to the ends of the solution column, an extrapolation was required to determine c_b and c_a. To perform this extrapolation, we needed to fit some suitable eqations to the data giving the equilibrium solute concentration as a function of r^2 or ξ where

$$\xi = (r_b^2 - r^2)/(r_b^2 - r_a^2) \quad (7)$$

For example, Richards and coworkers[9] used, for inhomogeneous or non-ideal systems, a least-squares quadratic fit over the ln c vs. r^2 data in the top and bottom third of the cell. We describe in the next paragraph the procedure for selecting the equations that were fitted to the data.

A polynomial in ξ,

$$\sum_0^n a_n \xi^n$$

was fitted to the data of ln c or c vs. ξ with the use of the least-squares method. To evaluate the number of terms necessary to fit ln c vs. r^2 data adequately, Richards and coworkers[9] allowed n to vary from 1 to 5. They concluded that in all cases the data were adequately represented by a cubic equation, as determined by the fact that the average deviation did not decrease for higher values of n. In our work, we allowed n to vary from 1 to 4 and found that in all cases the ln c or c vs. ξ data were adequately represented by a polynomial with n no greater than 3, as judged by the fact that the residual standard deviation did not decrease significantly for higher values of n. Since our purpose was to obtain the extrapolated value at $\xi = 0$ or $\xi = 1$, in choosing the equation to represent the data we impose an additional constraint: that the departure of the data from the fitted equation must not be systematic near $\xi = 1$ or $\xi = 0$. Thus, guided by a plot of the residual vs. ξ, we chose from the polynomials that give substantially the same residual standard deviation the one showing no systematic departure from the data near $\xi = 0$ or $\xi = 1$.

Of the ln c or c vs. ξ data, those obtained at radial positions too close to the top or the bottom of the solution column ($\xi = 1$ or $\xi = 0$) were distorted by the menisci and therefore must be deleted. The deletion of the data was accomplished in two steps. First, a plot of c vs. the radial position was made. Guided by the plot thus obtained, we deleted the points near $\xi = 1$ or $\xi = 0$ that departed distinctly from the trend established by the rest of the data. In the second step, a set of data near the top (or the bottom) with $0.75 < \xi < 1$ (or $0 < \xi < 0.25$) was fitted to a polynomial in the manner described in the last paragraph. Then, a subset obtained from the set by deleting three points nearer to the top (or the bottom) was similarly fitted to another polynomial. If the values of c at $\xi = 1$ (or $\xi = 0$) predicted by the two equations were not significantly different, no additional deletion of the data was made. However, if the two predicted values are significantly different, these three points were deleted from the ln c or c vs. ξ data and the second step was repeated. In general, the number of points in the set was about 70 and the second step was carried out at most twice.

Of the c vs. ξ data, a set of points near the top of the solution columns where $0.67 \sim \xi_l < \xi < 1$ was fitted to a polynomial chosen in the manner previously described. The polynomial was then used to calculate c_a, the value of c at $\xi = 1$. Similarly, from a set of points near the bottom of the solution column where $0 < \xi < \xi_u \sim 0.33$, we determine c_b, the value of c at $\xi = 0$. The values of c_b and c_a were also determined for $\xi_l = 0.75$, $\xi_u = 0.25$ and for $\xi_l = \xi_u = 0.5$. The results obtained with these pairs of values for ξ_u and ξ_l agreed with one another.

Using the conservation-of-mass condition,

$$\int_0^1 c(\xi)\mathrm{d}\xi = c_0 \quad (8)$$

we calculate the ln c vs. ξ data in the manner described by Richards and coworkers[9]. We then use these data to calculate, in the manner described for the treatment of the c vs. ξ data, the values of ln c at the top and the bottom of the solution column. The values of c_b and c_a thus obtained agreed with those obtained from the c vs. ξ data. *Figures 2* and *3* give typical plots of $\Delta c/c_0$ vs. ξ and $\ln(c/c_0)$ vs. ξ for a single run, where Δc is $c(\xi)$ less the value of c at $\xi = 0.97$. density difference $(\rho_2 - \rho_1)$ between two samples is given

RESULTS AND DISCUSSION

Partial specific volume

The partial specific volume is given by[10]

$$\bar{v} = V_{sp} + (1 - W_2)(\delta V_{sp}/\delta W_2) \quad (9)$$

where V_{sp} is the specific volume of the solution and W_2 is the weight fraction of the solute in the solution. At lower concentrations where the specific volume is linear in W_2, equation (9) reduces to

$$(\rho - \rho_0)/\rho = (1 - \bar{v}\rho_0)W_2 \quad (10)$$

where ρ is the density of the solution.

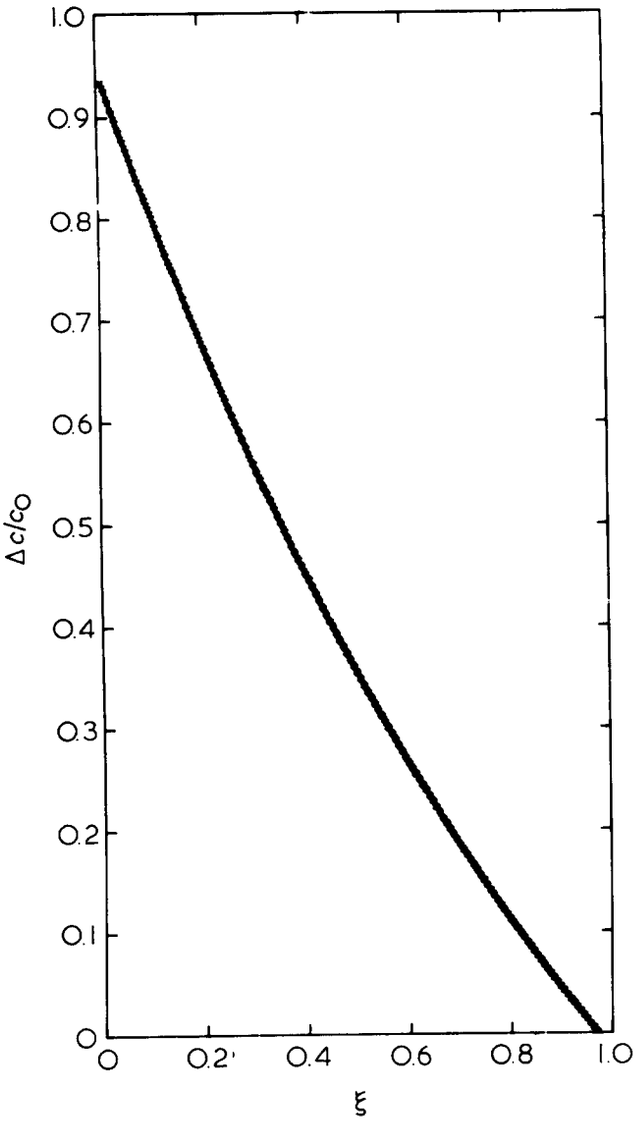

Figure 2 Typical plot of $\Delta c/c_0$ vs ξ

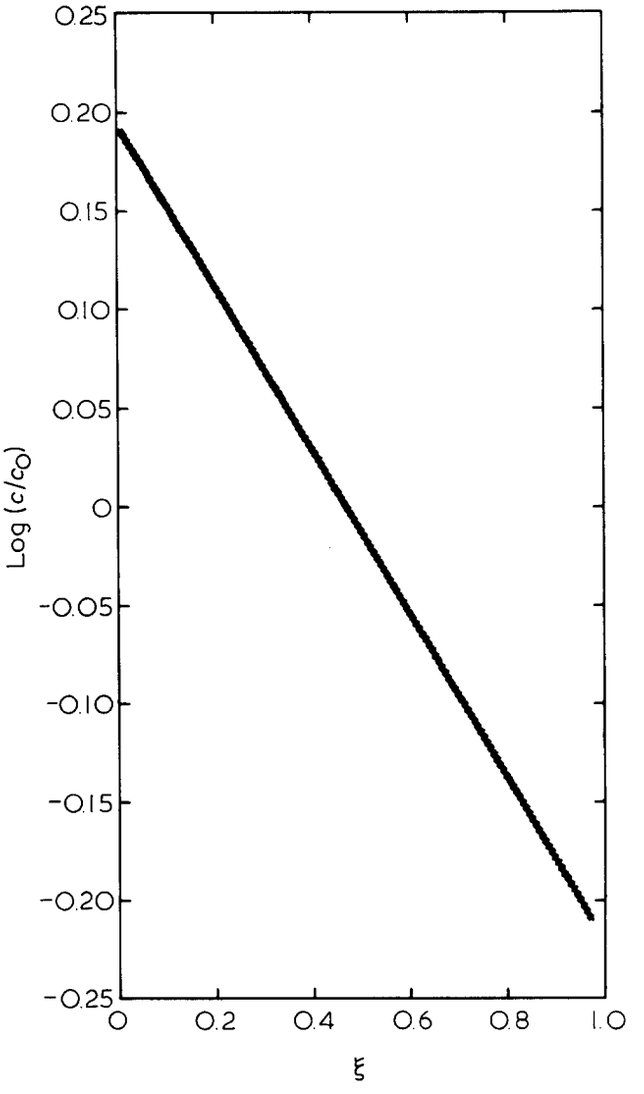

Figure 3 Typical plot of $\ln(c/c_0)$ vs ξ

The weight fractions of the ten solutions used in partial specific volume determination ranged from 0.0013 to 0.013. For these solutions, the specific volume was linear in W_2. Therefore, we fitted by least squares the observed values of $(\rho-\rho_0)/\rho$ to equation (10) and determined $\bar{v}$ from the slope $(1-\bar{v}\rho_0)$. A value of $0.932\,cm^3\,g^{-1}$ with a standard deviation of $0.0007\,cm^3\,g^{-1}$ was obtained for $\bar{v}$.

We now consider the likely sources of systematic error in the estimate of $\bar{v}$ and try to set upper limits on their magnitudes. For the density meter used in this work, the density difference $(\rho_2-\rho_1)$ between two samples is given by

$$\rho_2-\rho_1=A(T_2^2-T_1^2) \tag{11}$$

where T_2 and T_1 are the respective resonant period readings of the two samples. Since the constant A was determined by measuring the resonant periods for the xylene sample and the heptane sample, the errors in their densities led to a systematic error in $(\rho-\rho_0)$. In addition, the error in the density value for the solvent led to a systematic error in $(\rho-\rho_0)/\rho$ as well as ρ_0 in the factor $(1-\bar{v}\rho_0)$. Assuming that the uncertainties in these density readings were 50 ppm and that there were no mutual cancellations of errors, we obtained $\pm 0.0003\,cm^3\,g^{-1}$ as an estimate of the systematic error in $\bar{v}$. Adding these systematic errors and the standard deviation of the fit, we obtained a value of $\pm 0.001\,cm^3\,g^{-1}$ as the estimated error in $\bar{v}$.

Weight-average molecular weight

Table 1 gives the results of sedimentation equilibrium experiments for nine solutions of SRM 1478 polystyrene ranging in concentration from approximately $0.001\,g\,cm^{-3}$ to $0.005\,g\,cm^{-3}$. *Table 2* gives the experimental conditions and other constants that enter equation (6). In *Table 2*, r_1 and r_2 are the radial distances from the centre of the rotor to the inner and outer reference edges of the counterbalance. When the measured values of M_w^* were fitted by the unweighted least-squares method to a polynomial in the first power of J_0, as suggested by equation (5), we obtained from the intercept a value of $37.4\,kg\,mol^{-1}$ for M_w with a standard deviation of $0.26\,kg\,mol^{-1}$. Also obtained was a value of -0.02 kg/(mol. fringe) for the slope of the polynomial with a standard deviation of 0.02 kg/(mol. fringe).

We now consider the likely sources of systematic error in the estimate of M_w and try to set upper limits on their magnitudes. The results of our analysis are given in *Table 3* where $r_h=(r_1+r_2)/2$ with r_1 and r_2 the actual radial

distances of the inner and outer reference edges of the counterbalance, and R_a and R_b are, respectively, the radial distances, on the interference photograph, of the top and the bottom of the liquid column.

Some sources of systematic error deserve additional comments. We consider the contributions of a few sources to the systematic error in the quantity $(r_b^2 - r_a^2)$. We determined r_b and r_a with the use of the relation

$$r_u = r_h + (r_2 - r_1)(R_u - R_h)/(R_2 - R_1) \quad (12)$$

with

$$u = a \text{ or } b$$

and

$$R_h = (R_2 + R_1)/2$$

where R_2 and R_1 are, respectively, the radial distances, on the interference photograph, of the inner and outer reference edges of the counterbalance. Using equation (12) we estimated the contributions from r_h and $(r_2 - r_1)$ to the systematic error in $(r_b^2 - r_a^2)$ and thence in M_w.

The widths of the images of the air–solution meniscus and the solution–water meniscus on the interference photograph were both about 100 μm. The value of M_w was obtained with the assumption that the meniscus was at the position where the optical density of its image was minimum. If we assumed the miniscus to be located at one-third the width of the image from the outermost edge of the image[8,11], we obtained a value of M_w larger than the one reported here by 0.2%. The fractional error in M_w due to the errors δr_a and δr_b in r_a and r_b is given by

$$\frac{\delta M_w}{M_w} = \frac{2r_b[m_b - (c_b - c_a)]\delta r_b + 2r_a[(c_b - c_a) - m_a]\delta r_a}{(r_b^2 - r_a^2)(c_b - c_a)} \quad (13)$$

where m_b and m_a are, respectively, the value of $(dc/d\xi)$ at the top and the bottom of the liquid column. Since the air–solution meniscus and the solution–water meniscus are both concave towards centrifugal direction when the organic solvent is lighter than water[11], δr_a and δr_b likely had the same sign. If we assumed that δr_a and δr_b had the same sign, an estimated systematic error of 20 μm in R_a and in R_b contributed to a systematic error of 0.3% in M_w, while the same error in R_a and in R_b led to a systematic error of 0.9% if we assumed that δr_a and δr_b were not correlated. The average of these two values was taken to be an estimate of the systematic error in M_w due to the errors in R_a and R_b.

The sum of the absolute values of the individual contributions given in *Table 3* gives an estimated total error of 1.1% while the root-sum-square of these contributions gives an estimated total error of 0.7%. We believe that the first method gives an overly pessimistic estimate of total error. We therefore take 0.9%, the average of these two estimates, as our estimate of the total systematic error. Finally, to take account of any sources of error not explicitly considered here, we add 1.1% and give 2% as the expected limit of systematic error from all sources, including sources not recognized and treated here.

Table 1 Apparent weight-average molecular weight from sedimentation equilibrium experiments

Run	J_0 (fringes)	M_W^* (kg mol^{-1})
3260	3.65	37.52
3277	4.68	37.50
3266	7.22	36.71
3274	7.24	37.32
3270	10.97	37.04
3262	11.06	36.88
3268	14.34	37.38
3272	18.78	37.40
3264	19.02	36.64

Table 2 Experimental conditions and constants

ω (rpm)	10006
T (K)	308.15
ρ_0 (g cm^{-3})	0.76311
$\bar{v}$ (cm^3 g^{-1})	0.932
r_1 (cm)	5.7046
r_2 (cm)	7.2954

Table 3 Systematic error in M_W

Source of systematic error	Magnitude of error	Error in M_W (%)
T (K)	±0.1	±0.03
ω (rpm)	±1	±0.02
r_h (cm)	±0.006	±0.08
$(r_2 - r_1)$ (cm)	±0.0005	±0.03
ρ_0 (g cm^{-3})	±0.0001	±0.03
$\bar{v}$ (cm^3 g^{-1})	±0.001	±0.3
R_a, R_b (μm)	±20	±0.6

SUMMARY

In conclusion, we have described in detail the determination of the weight-average molecular weight of SRM 1478 polystyrene by sedimentation equilibrium method. We have also described a new method to analyse, with the use of a commercial image digitizer, the ultracentrifugation data recorded in the form of Rayeligh interference pattern. From the analysis of our data, we have obtained for the SRM 1478 polystyrene a weight-average molecular weight of 37 400 g mol^{-1} having a sample standard deviation of 0.7% with seven degrees of freedom and an expected limit of systematic error of 2%.

ACKNOWLEDGEMENTS

We thank J. J. Filliben, R. A. Kirsch, P. H. Verdier, J. R. Whetstone and S. C. Greer for helpful discussions. We thank J. R. Maurey and R. E. Lowry for experimental assistance.

REFERENCES

1 Svensson, H. *Acta Chem. Scand.* 1951, **5**, 1301
2 Billick, I. H. and Bowen, R. J. *J. Phys. Chem.* 1965, **69**, 4024
3 Maurey, J. R. unpublished results
4 Richards, E. G., Teller, D. C. and Schachman, H. K. *Anal. Biochem.* 1971, **41**, 189
5 Richards, E. G., Teller, D. C., Hoagland, V. D., Jr, Haschemeyer, R. H. and Schachman, H. K. *Anal. Biochem.* 1971, **41**, 215
6 Bowman, H. A., Schoonover, R. M. and Carroll, C. L. *J. Res. Natl. Bur. Stand. A* 1974, **78**, 13
7 Bowman, H. A., Schoonover, R. M. and Carroll, C. L. *Metrologia* 1974, **10**, 117
8 Albright, D. A. and Williams, J. W. *J. Phys. Chem.* 1967, **71**, 2780
9 Richards, E. G., Teller, D. C. and Schachman, H. K. *Biochemistry* 1968, **7**, 1054
10 McIntyre, D., Wims, A., Williams, L. C. and Mandelkern, L. *J. Phys. Chem.* 1962, **66**, 1932
11 Erlander, S. R. and Babcock, G. E. *Biochim. Biophys. Acta* 1961, **50**, 205